COMPUTATIONAL FLUID DYNAMICS ANALYSIS ON HEAT TRANSFER AND FRICTION FACTOR CHARACTERISTICS OF A TURBULENT FLOW FOR INTERNALLY GROOVED TUBES

by

Ponnusamy SELVARAJ, Jagannathan SARANGAN, and Sivan SURESH *

Department of Mechanical Engineering, National Institute of Technology, Tiruchirapalli, India

Original scientific paper
DOI: 10.2298/TSCI110404010S

The article presents computational fluid dynamics studies on heat transfer, pressure drop, friction factor, Nusselt number and thermal hydraulic performance of a plain tube and tube equipped with the three types of internal grooves (circular, square and trapezoidal). Water was used as the working fluid. Tests were performed for Reynolds number ranges from 5000 to 13500 for plain tube and different geometry inside grooved tubes. The maximum increase of pressure drop was obtained from numerical modeling 74% for circular, 38% for square, and 78% for trapezoidal grooved tubes were compared with plain tube. Based on computational fluid dynamics analysis the average Nusselt number was increased up to 37%, 26%, and 42% for circular, square and trapezoidal grooved tubes, respectively, while compared with the plain tube. The thermal hydraulic performance was obtained from computational fluid dynamics analysis up to 38% for circular grooved tube, 27% for square grooved tube and 40% for trapezoidal grooved tube while compared with the plain tube.

Key words: *heat transfer enhancement)/augmentation, grooved tubes, friction factor, computational fluid dynamics, modeling and numerical simulation*

Introduction

Heat transfer enhancement techniques can be divided into two categories passive and active. In passive heat transfer enhancement an object which does not use external energy, such as groove inside the tube, has the duty of increasing the heat transfer rate. Forced convection heat transfer is the most frequently employed mode of the heat transfer in heat exchangers or in various chemical process plants. During the last two decades, computational fluid dynamics (CFD) has become a very powerful tool in the process of industries not only for the research and development of new processes but also for the understanding and optimization of existing one. Pressure drop and heat transfer predictions often are accurate even in complex geometries. Thus CFD has become the state of the art in thermal engineering like in heat exchanger design. Aubin *et al.* [1] investigated the effect of the modeling approach, discretization and turbulence model on mean velocities and turbulent kinetic energy and global quantities such as the power and circulation numbers. The results have been validated by laser Doppler velocimetry data. Rahimi *et al.* [2] reports experimental and CFD investigations on friction factor, Nusselt number and thermal hydraulic performance of a tube equipped with the classic and three modified

* Corresponding author; e-mail: ssuresh@nitt.edu

twisted tape inserts. Uses of the artificial grooved tubes are widely used in modern heat exchangers, because they are very effective in heat transfer augmentation.

Bilen *et al.* [3] experimentally investigated the surface heat transfer and friction characteristics of a fully developed turbulent air flow in different grooved tubes. Tests were performed for Reynolds number range of 10000 to 38000 and for different geometric grooved shape (circular, trapezoidal, and rectangular) tubes.

Kumar and Saini [4] presents the performance of a solar air heater duct provided with artificial roughness in the form of a thin circular wire in arc shaped geometry has been analyzed using CFD. The effect of arc shaped geometry on heat transfer coefficient, friction factor, and performance enhancement were investigated covering the range of roughness parameter (from 0.0299 to 0.0426) and working parameter (Re from 6000 to 18000). Different turbulent models have been used for the analysis and their results were compared. Renormalization group (RNG) k-ε model based results have been found in good agreement and accordingly this model was used to predict heat transfer and friction factor in the duct.

Xiong and Chung [5] analyzed with the help of CFD solver to isolate the roughness effect and solve the 3-D Navier-Stokes equations for the water flow through the general rough micro tubes with diameter $D = 50$ m and length $L = 100$ m. The model has a potential to be used for direct simulations of 3-D surface roughness effects on the slip flow. Craft *et al.* [6] reports computations of the fluid and heat transfer from a row of round jets impinging onto a concave semicircular surface designed to reproduce important flow features found in internal turbine blade cooling applications. Iacovides *et al.* [7] discussed the results of a combined experimental and numerical study of flow and heat transfer in a straight duct, with ribs of square cross-section along the two opposite walls, in a staggered arrangement and at an angle of 45º to the main flow direction. Chaube *et al.* [8] studied a computational analysis of heat transfer augmentation and flow characteristics due to artificial roughness in the form of ribs on a broad, heated wall of rectangular duct for turbulent flow has been carried out. Karagoz and Kaya [9] presents CFD investigation of the flow field and heat transfer characteristics in a tangential inlet cyclone which is mainly used for the separation of a two phase flow. Finite volume based Fluent® software was used and the RNG k-ε turbulence model was adopted for the modeling highly swirling turbulent flow. Rigby and Evans [10] reports single and multiphase flow dynamics around bluff bodies in liquid cross-flows have been investigated using CFD modeling. Li *et al.* [11] investigated the periodicities of convection heat transfer in channels with periodically grooved parts are studied numerically using an unsteady state model. The governing equations are discretized using SIMPLE algorithm with QUICK scheme.

Eiamsa-Ard *et al.* [12] presents the applications of a mathematical model for simulation of the swirling flow in a tube induced by loose – fit twisted tape insertion. Zimparov [13, 14] investigated a simple mathematical model following the suggestions of Smithberg and Landis has been created to predict the friction factors for the case of a fully developed turbulent flow in a spirally corrugated tube combined with a twisted tape insert. Goto *et al.* [15, 16] investigated the condensation and evaporation heat transfer of R410A inside internally grooved horizontal tubes. The measured local pressure drop, heat transfer coefficients were compared with the predicted values from previous correlations proposed by the authors.

Promvonge [17] investigated that the snail entry with the coiled square-wire provides higher heat transfer rate than that with the circular tube of under the same conditions. Promvonge [18] studied thermal augmentation in circular tube with twisted tape and wire coil turbulators. Also he presents that heat transfer enhancement can create one or more combinations of the following conditions that are favorable for the increase in heat transfer rate with an

undesirable in increase in friction: (1) Interruption of boundary layer development and rising degree of turbulence (2) increase in heat transfer area (3) generating of swirling and/or secondary flows. To date, several studies have been focused on passive heat transfer enhancement methods reverse/swirl flow devices (rib, groove, wire coil, conical ring snail entry, twisted tape, winglet, *etc*.,) form an important group of passive augmentation technique.

Chiu and Jang [19] numerical and experimental analyses were carried out to study thermal hydraulic characteristics of air flow inside a circular tube with different tube inserts. Zhang *et al.* [20] experimental study on evaporation heat transfer of R417A flowing inside horizontal smooth and two internally grooved tubes with different geometrical parameters were conducted with the mass flow rate range from 176 to 344 kg/s. Based on the experimental results, the mechanism and mass flow rate, heat flux, vapor quality and enhanced surface influencing the evaporation heat transfer co-efficient were analyzed and discussed.

Li *et al.* [21] studied the turbulent heat transfer and flow resistance in an enhanced heat transfer tube, the DDIR tube, were studies experimentally and numerically, water was used as the working fluid with Re between 15000 and 60000. The numerical simulations solved the 3-D Reynolds-averaged Navier-Stokes equations with the standard k-ε model in the commercial computational fluid dynamics code, Fluent. The numerical results agree well with the experimental data, with the largest discrepancy of 10% for the Nusselt numbers and 15% for friction factors.

Karwa *et al*. [22] carried out an experimental investigation of heat transfer and friction for the flow of air in rectangular ducts with repeated rib roughness on a broad wall. Friction factor and heat transfer coefficient correlations have been developed based on the law of wall similarity and heat-momentum transfer analogy. Karwa [23] presents results of an experimental investigation of heat transfer and friction in rectangular ducts with repeated rectangular cross--section ribs on one broad wall in transverse, inclined, v-continues and v-discrete pattern. Tanda [24] carried out an experimental study on heat transfer in a rectangular channel with transverse and V-shaped broken ribs. Local heat transfer coefficients were obtained at various Reynolds numbers within the turbulent flow regime. Vicente *et al.* [25] carried out experimental study on corrugated tubes in order to obtain their heat transfer and isothermal friction characteristics. The use of water and ethylene glycol as test fluids has allowed covering a wide range of turbulent fluid flow conditions. Reynolds number from 2000 to 90000 and Prandtl number from 2.5 to 100. Helical-wire-coils fitted inside a round tube have been experimentally studied in order to characterize their thermodynamic behavior in laminar, transition and turbulent flow. Experimental correlations of Fanning friction factor and Nusselt number as functions of flow and dimensionless geometric parameters have been proposed by Garcia *et al.* [26].

In the present study the pipe flow with three types of grooved tubes (circular, square, trapezoidal) at constant wall flux condition was studied numerically for Reynolds number ranges from 5000 to 13500 and groove depth was fixed to investigate the effect of the groove shapes on heat transfer. The thermal hydraulic performance for all the cases was also performed. The present work a CFD modeling was carried out in order to find out the heat transfer in a tube equipped with grooves.

Detailed geometry of grooved tubes

The present CFD analysis a plain carbon steel tube with 38.14 mm was selected since, it is a standard size pipe used in boiler heat transfer equipments. It has an internal diameter 38.14 mm and thickness of 5.060 mm. A depth of 4 mm was chosen for grooves because of their pipe thickness is 5.060 mm. In order to investigate the effect of grooved shapes in a carbon steel tube on

heat transfer and friction factors, three different grooved tubes and plain tube were used for the present analyses. Three different geometrical grooved tubes are shaped as circular, square, and trapezoidal are shown in fig. 1. The depth and length of circular and trapezoidal grooves were fixed as 4 mm and 8 m, respectively. The depth and length of square groove is 4 mm each. The same number of grooves (n = 93) were designed for all the three geometries, because of the fixed pitch length is 16 mm.

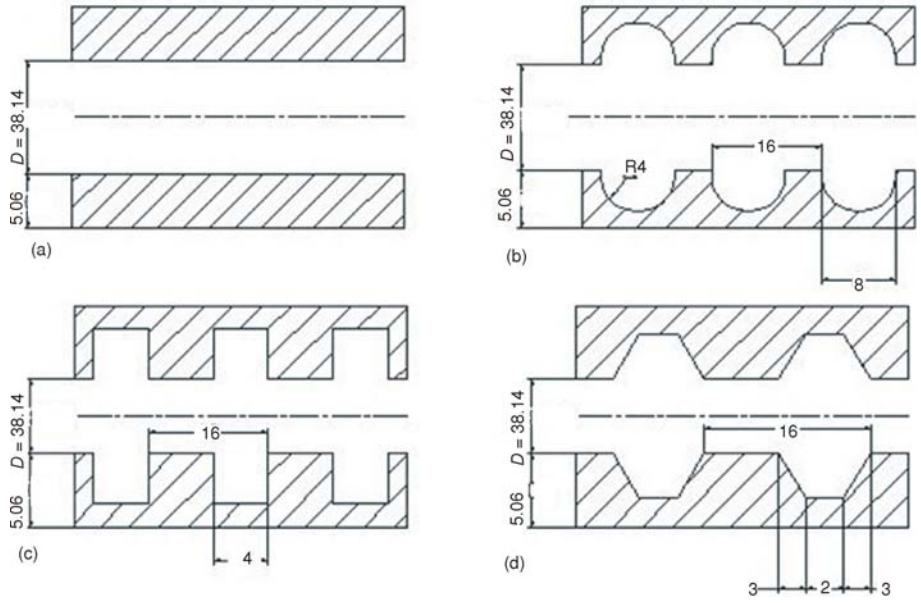

Figure 1. The geometric shapes of the grooved tubes in mm; (a) plain tube, (b) circular grooved tube, (c) square grooved tube, and (d) trapezoidal grooved tube

Theory and development of CFD modeling

The net heat transfer rate from the inner tube surface to the fluid flow passing through the test tube by convection can be calculated subtracting heat losses from the total electrical power input at the steady state conditions [3, 27]. The net rate heat transfer is also equal to the rate of the heat transfer given to the fluid passing through the test section, using inlet and outlet temperature difference and mass flow rate [28].The energy balance equation can be written as:

$$q_{\text{net}} = q_{\text{vol}} - q_{\text{loss}} = mC_p\,(T_{\text{o}} - T_{\text{i}}) \tag{1}$$

where q_{net} is the net heat transfer rate given to the fluid inside the test tube, q_{vol} (= V^2/R) is the measured electrical power input to the heater, and q_{loss} denotes all the heat losses from the test section.

On the other hand, the heat transfer to the cold fluid that surrounds the tube may be approximated by:

$$q = hA(T_{\text{w}} - T_{\text{b}}) \tag{2}$$

where

$$T_{\text{b}} = \frac{T_{\text{o}} + T_{\text{i}}}{2} \quad \text{and} \quad T_{\text{w}} = \frac{\sum T_{\text{w}}}{5} \tag{3}$$

Using eqs. (1) and (2), the convection heat transfer co-efficient on the grooved tube wall at the steady rate can be calculated by:

$$h = \frac{mC_p(T_o - T_1)}{A(T_w - T_o)} \tag{4}$$

where A is the inner surface area of the smooth tube, T_o and T_i are outlet and inlet temperatures of water flow, respectively, and T_w is the average temperature of the locations along the tube surface.

In all the calculations the smooth surface was taken as the heat transfer area. The average Nusselt number is calculated as [29]:

$$\mathrm{Nu}_m = \frac{hD}{K} \tag{5}$$

The Reynolds number is based on the average flow inlet velocity and the tube inlet diameter [29]:

$$\mathrm{Re} = \frac{VD}{\nu} \tag{6}$$

In a fully developed tube flow the friction factor (f) can be determined by measuring the pressure drop across the test tube length as:

$$f = \frac{\Delta P}{\frac{L}{D}\left(\rho\frac{V^2}{2}\right)} \tag{7}$$

where ΔP is the pressure drop across the test tube measured by an electronic transmitter, L – the test tube length, and V – the mean water velocity at the entrance of the test section which was calculated from volumetric flow rate divided by the cross-section area of the tube. D is the inner diameter of the test tube at the inlet. The value of the thermophysical properties of water were evaluated at the bulk fluid temperature $T_b = T_o + T_i$

CFD modeling

In this investigation a 3-D numerical simulation of the conjugate heat transfer was conducted using the CFD code FLUENT ® [30]. The CFD modeling involves numerical solutions of the conservation equations for mass, momentum and energy. These three equations are used to model the convective heat transfer process with the following assumptions, (a) steady 3-D fluid flow and heat transfer, (b) incompressible fluid and flow, and (c) physical properties of hot fluid are temperature dependent.These equations for incompressible flows can be written as follows:

– *mass conservation*

$$\frac{\partial\rho}{\partial t} + \nabla(\rho\vec{u}) = 0 \tag{8}$$

– *momentum conservation*

$$\frac{\partial(\rho\vec{u})}{\partial t} + \nabla(\rho\vec{u}\vec{u}) = \rho g - \nabla P + \nabla(\bar{\bar{\tau}}) \tag{9}$$

– *energy conservation*

$$\frac{\partial(\rho e)}{\partial t} + \nabla[\vec{u}(\rho e + P)] = \nabla[K_{\mathrm{eff}}\nabla T + (\bar{\bar{\tau}}_{\mathrm{eff}}\vec{u})] \tag{10}$$

where

$$\bar{\bar{\tau}} = \mu\left[(\nabla\vec{u} + \nabla\vec{u}^{\,T}) - \frac{2}{3}\nabla\vec{u}\vec{I}\right] \tag{11}$$

In the case of turbulent flow, the random nature of flow precludes computations based on a complete description of the motion of all the fluid particles. Turbulent flows are characterized by fluctuating velocity fields. These fluctuations mix the transported quantities such as momentum and energy in terms of small scale and high frequency. Therefore, turbulent flows are too computationally expensive to be simulated in practical calculations. On the other hand, the instantaneous exact governing eqs. (8)-(10) could be averaged in time and in space or otherwise manipulated to remove these small scales, resulting in a modified set of equations are computationally easier to solve. However, the modified equations contain additional unknown variables and additional turbulence equations are needed to determine these variables in terms of known quantities. In the present study, the renormalization group (RNG) version of *k*-*ε* turbulence model with enhanced wall functions for the near wall treatment was used to model the turbulent flow regime. The following equations are used for this purpose.

$$\mu_{\text{eff}} = \mu + \mu_{\text{t}}, \quad \mu_{\text{t}} = \rho C_{\mu} \frac{k^2}{\varepsilon} \tag{12}$$

$$\frac{\partial(\rho k)}{\partial t} + \frac{\partial}{\partial x_i}(\rho k u_i) = \frac{\partial}{\partial x_i}\left(\frac{\mu}{\sigma_{\text{k}}}\frac{\partial k}{\partial x_{\text{i}}}\right) + \mu_{\text{t}}\left(\frac{\mu_{\text{eff}}}{\sigma_{\text{k}}}\frac{\partial k}{\partial x_i}\right) + \mu_{\text{t}}\left(\frac{\partial u_i}{\partial x_j} + \frac{\partial u_j}{\partial x_i}\right)\frac{\partial u_i}{\partial x_j} - \rho\varepsilon \tag{13}$$

$$\frac{\partial(\rho\varepsilon)}{\partial t} + \frac{\partial}{\partial x_{\text{i}}}(\rho\varepsilon u) = \frac{\partial}{\partial x_{\text{i}}}\left(\frac{\mu_{\text{eff}}}{\sigma_{\text{k}}}\frac{\partial \varepsilon}{\partial x_{\text{i}}}\right) + C1\varepsilon\frac{\varepsilon}{K}\mu_{\text{t}}\left(\frac{\partial u_i}{\partial u_j}\frac{\partial u_j}{\partial x_i}\right)\frac{\partial u_i}{\partial u_j} - C2\varepsilon\frac{\varepsilon^2}{k} - \alpha\rho\frac{\varepsilon^2}{k} \tag{14}$$

$$\alpha = C_{\mu}\eta^3\frac{1-\dfrac{\eta}{\eta_0}}{1+\beta\eta^3}, \quad \eta = E\frac{k}{\varepsilon}, \quad E^2 = 2E_{ij}E_{ij} \quad E_{ij} = 0.5\left(\frac{\delta u_i}{\delta x_j} + \frac{\delta u_j}{\delta x_i}\right) \tag{15}$$

Geometry and grid arrangement

The geometry and the grid were generated using GAMBIT® the preprocessing module of the FLUENT 6.3. The geometry and the grid for plain tube, circular grooved tube, square grooved tube and trapezoidal grooved tube are created separately in GAMBIT and imported into FLUENT. Figure 2(a) shows the grid for the plain tube configuration for turbulent flow. A boundary layer mesh is created near the wall to capture the wall effects in FLUENT. Because of the complexity of physical model with respect to the computational domain, it is difficult to use a single structural mesh in the entire domain. The whole computational domain is thus divided into several sub-domains. The mesh is a quadrilateral face mesh and it is swept through the volume of the cylinder. The volume is meshed by hexahedral cell with interval size 3. Figures 2(b), 2(c) and 2(d) shows the grid generation for circular, square and trapezoidal grooved tubes for turbulent flow. The volume has to be split or divided suitably so that one can get a hexahedral mesh. Here also boundary layer is used to predict the flow near wall regions.

The CFD model was made of 2D-axi-symmetry model, since the domain is a pipe. Suitable development lengths were given to nullify the effects of the boundary conditions. The mesh is of good quality quadrilateral meshes with boundary layers at the wall region to predict the wall effects exactly. Mesh was refined in two steps and the results were checked. The results showed no change to the previous mesh step. So, a grid independence test was conducted and the final mesh results were presented in the report. The details for the CFD model and mesh are given below.

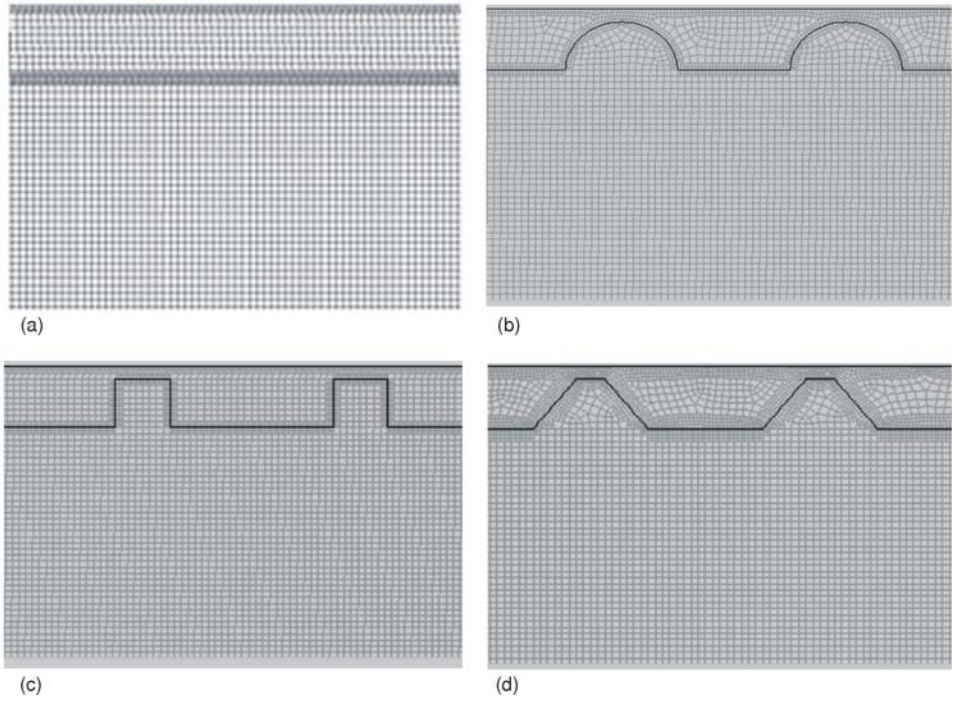

Figure 2. (a) Plain tube, (b) circular grooved tube, (c) square grooved tube, (d) trapezoidal grooved tube

Number of cells is for 1st mesh 120858, 2nd mesh 180200, 3rd and for final mesh 220800. Since a boundary mesh to resolve the near wall region and a good quality quadrilateral mesh is used in the model the results are near reality.

Boundary conditions

The boundary zone location is specified in the GAMBIT itself; the inlet, outlet and the wall condition location is specified. To make the flow fully developed 2.14 m length of pipe is provided before the test section at the inlet and outlet of the pipes for plain, circular, square and trapezoidal grooved tubes for both laminar and turbulent flow.

Fluid entry boundary condition

The mass flow inlet boundary conditions are 20 litres per minute with constant heat flux of 9699.6 W/m^2.

Fluid exit boundary condition

The outlet boundary condition of pressure outlet was prescribed as the pipe outlet. The pressure outlet conditions require a numerical value for the relative static (gauge) pressure at the outlet boundary. This value was set to zero, *i. e*. assumed to be at atmospheric pressure. All other conditions associated with velocities at the pressure outlet boundaries were extrapolated from the interior of the computational domain.

Wall boundary condition

The pipe wall is provided with wall boundary condition, a constant heat flux is provided for plain and grooved tubes. The rest of the boundary by default is wall boundary condition.

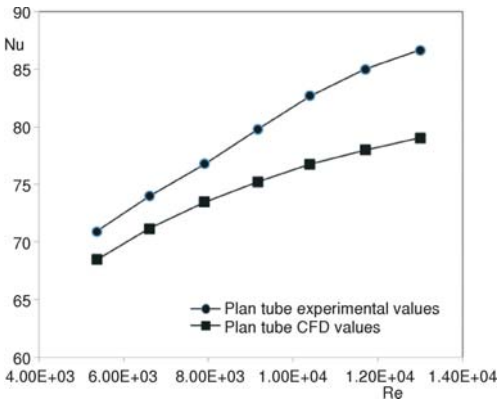

Figure 3. Validation of CFD results and experimental values for Nusselt number with plain tube

Results and discussion

Validation of plain tube

In fig. 3 the results obtained by computational fluid dynamics have been compared with experimental values for Nusselt number for plain tube.

The average deviation of the experimental values with CFD values of Nusselt number is ±9%. It has been observed that the results obtained by Renormalization-group (RNG) k-ε model are in good agreement with experimental results. It is therefore, for the present numerical study (RNG) k-ε model has been employed to simulate the flow and heat transfer.

In fig. 4 the pressure drop results obtained by computational fluid dynamics have been compared with experimental values for plain tube. The average deviation of the experimental values with CFD values of pressure drop is ±6%.

In fig. 5 illustrate heat transfer co-efficient obtained by CFD have been compared with experimental values for plain tube. The average deviation of the experimental values with CFD values of heat transfer co-efficient is ±9%.

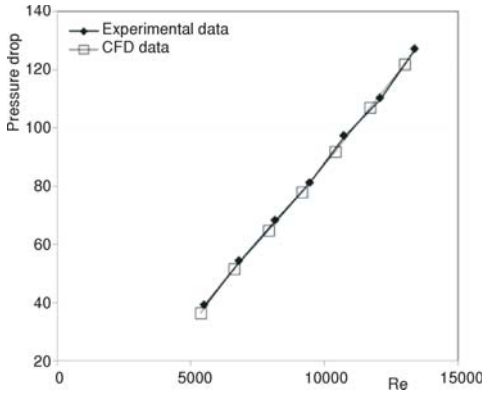

Figure 4. Validation of CFD results and experimental values of pressure drop for plain tube

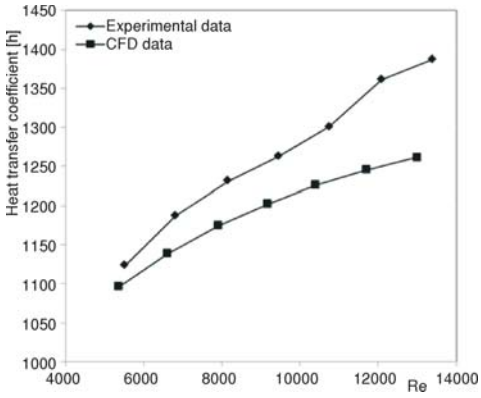

Figure 5. Validation of CFD results and experimental values of heat transfer coefficient for plain tube

CFD results

The change in temperature and pressure drop across the test tube at different inlet velocities for the plain and various grooved geometry tubes were obtained from the numerical

modeling. However, in general the pressure drop, had increased with any of the grooved tubes were used. In addition, the results show that for all fluid velocities the highest temperature obtained when the trapezoidal grooved tube was used although it caused more pressure drop. The whole results show that increased pressure drop and increased temperature ensures the increased heat transfer rate.

Figure 6 shows the velocity vector plots of various grooved tubes. Generally all the plots show similar flow patterns with a circulation loop at the inside of the groove of the tubes. However, some slight differences can be noticed. It is evident that the circulation increases the heat transfer rate by using grooved tubes.

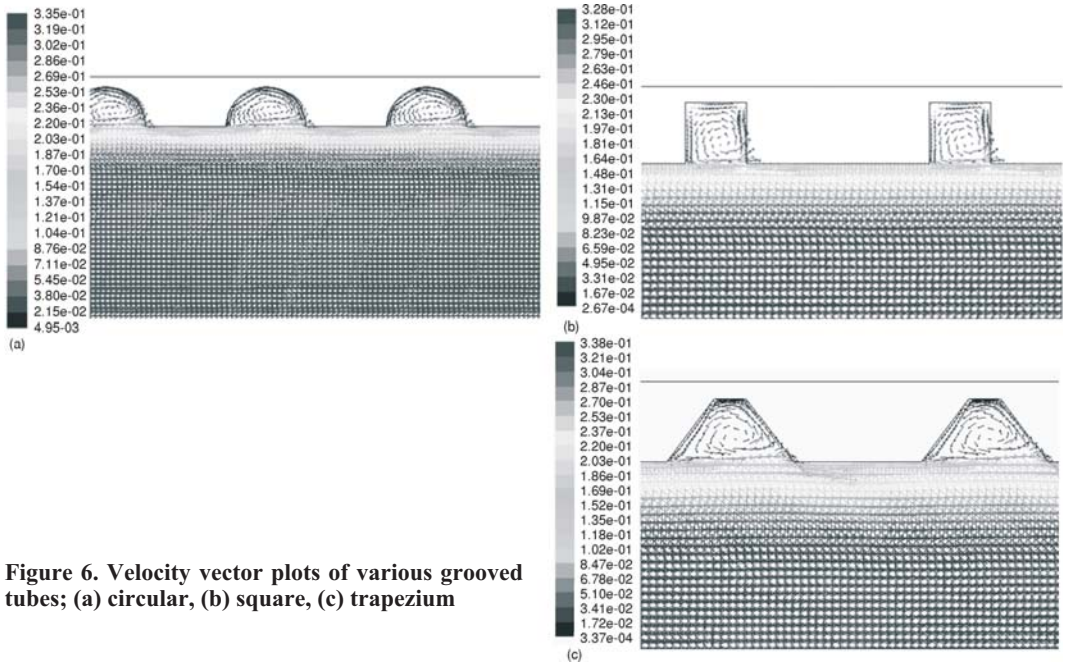

Figure 6. Velocity vector plots of various grooved tubes; (a) circular, (b) square, (c) trapezium

The square groove causes more turbulence intensity in the flow, because its sharp corner edge can produce more turbulence than the smooth surface, but, it causes more re-circulation region inside the groove. So, it prevents good mixing of the fluid. Thus, it results in less increase of heat transfer compare with both circular and trapezoidal grooved tubes. In conclusion, both circular and trapezoidal grooves causes more considerable enhancement in heat transfer due to more sweeping surface, good flow mixing and decrease of the re-circulation region as mentioned above [2, 3].

The local heat transfer co-efficient along the test tube with circular, square, and trapezoidal grooves were in the range of Reynolds number 5000 to 135000. From the CFD analysis, it is observed that, the heat transfer coefficient systematically increase as Reynolds number increases. The highest local heat transfer is in trapezoidal grooved tube (1503-1843 W/m^2K) and lowest is in square grooved tube (1299-1265 W/m^2K).The circular grooved tube value is 1439-1784 W/m^2K. It shows that augments the heat transfer performances in the grooved tubes are the intensification of the fluid mixing inside the tubes.

The CFD investigations of heat transfer for the smooth tube and grooved tubes (circular, square and trapezoidal) were analyzed. By referring to fig. 7 one can observe that as Reynolds number increases, Nusselt number also increases. The increase in Nusselt number indicates the increase of heat transfer co-efficient due to increase of convection. The results show that the calculated Nusselt number for trapezoidal grooved tube was highest among the plain and grooved tubes at all examined Reynolds numbers.

The variation of the friction factor with Reynolds number for the grooved tubes was illustrated in fig. 8. It is expected, the analyzed friction factors for the grooved tubes were significantly higher than that obtained for the plain tube. The maximum friction factor was obtained when the trapezoidal groove tube were employed. It can be seen that the friction factor decreases while increasing, the Reynolds number. For plain and grooved tube arrangements, it was found that the friction factor values were higher at lower Reynolds numbers.

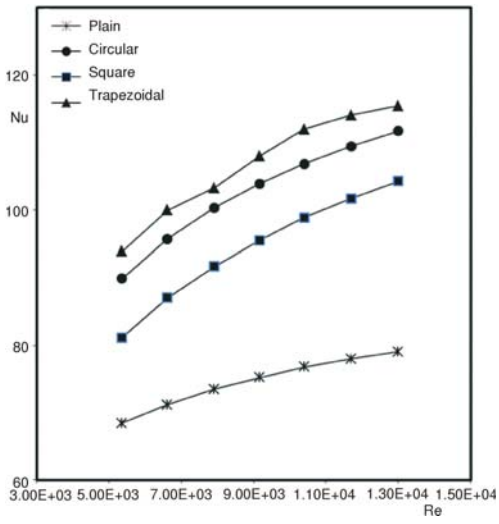

Figure 7. Nusselt number *vs*. Reynolds number for plain and various grooved tubes

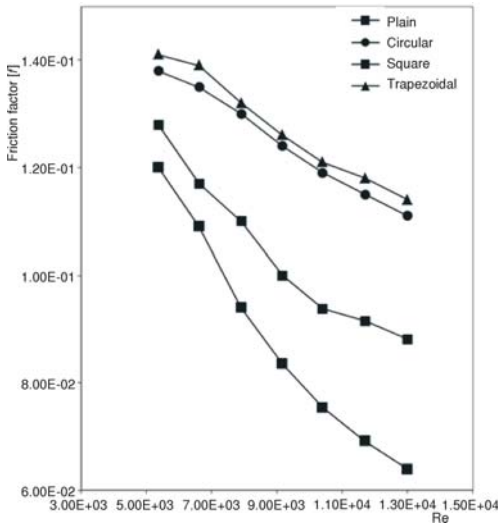

Figure 8. Friction factor *vs*. Reynolds number for plain and various grooved tubes

The effectiveness of heat transfer augmentation in the grooved tubes relative to the plain tube was compared in fig. 9. The effectiveness was indexed by the ratio of the Nusselt number of the grooved tube to that of the plain tube in terms of Nu/Nu_0.As shown in fig. 9 the Nu/Nu_0 ratio at different fluid flow rates was lower for the square grooved tube when compared to other grooved tubes. The results show that at some Reynolds numbers the reported values of Nu/Nu_0 for trapezoidal grooved tube were 54% more than that of plain tube.

In the present study the thermal hydraulic performance of the grooved tubes are calculated with the help of following equation:

$$\text{Thermal-hydraulic performance} = \frac{\dfrac{\text{Nu}}{\text{Nu}_0}}{\sqrt[3]{\dfrac{f}{f_0}}} \tag{17}$$

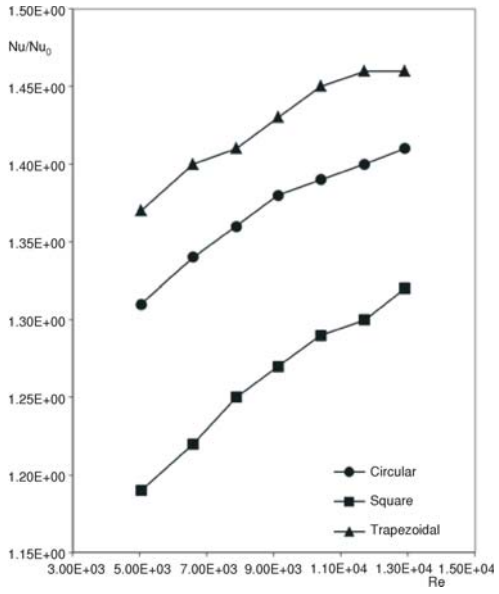

Figure 9. Effectiveness Nu/Nu_0 *vs.* Reynolds number for various grooved tubes

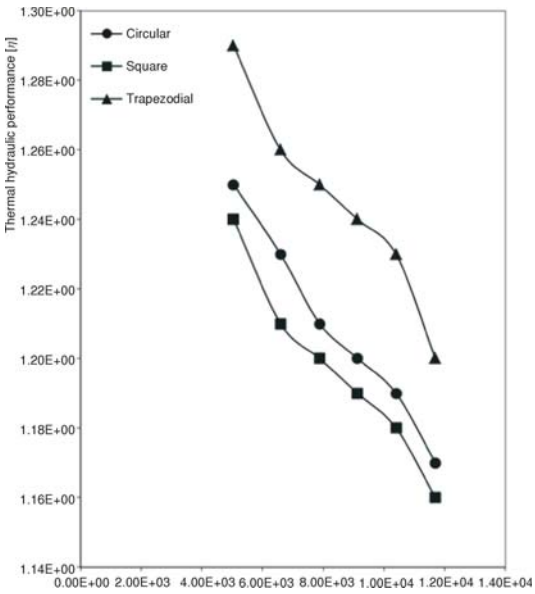

Figure 10. Thermal hydraulic performance *vs.* Reynolds number for various grooved tubes

The calculated performance ratios for different setups were compared in fig. 10. The figure shows that the performance ratio decreased while increasing the Reynolds number. This might indicate, at lower velocities the role of grooved tubes increasing the turbulence intensity was more significant at higher velocities [2]. It is observed that more deviation occurred at higher Reynolds numbers for CFD results. This can be explained by the weakness of the turbulence model in predicting the fluctuating properties at higher flow rates setup.

The results confirm that using any one of the above mentioned grooved tubes can increases the friction factor. The trapezoidal grooved tube obtained the highest friction factor while the lowest friction factor was obtained with the square grooved tube.

Conclusions

The Fluent® was used for modeling and CFD analysis in the present work. The different geometry grooved tube like circular, square and trapezoidal were introduced for this analysis. The CFD code might serve as a powerful tool to assess the heat transfer characteristics for turbulent flow inside the tubes.

The Nusselt number was increased and friction factor was decreased with increasing Reynolds number for all the tubes. It has been observed that RNG k-ε model results have been found to have good agreement with plain tube results. Based on CFD analysis, higher Nusselt number and thermal hydraulic performance were obtained for the trapezoidal grooved tube compared with plain and grooved tubes in the studied range of Reynolds number from 5000 to 13500.

Overall thermal hydraulic performance was obtained up to 26% higer for circular grooved tube, 24% for square grooved tube, and 30% for trapezoidal grooved tube in compared with plain tube. The higher turbulence intensity of the fluid close to the tube wall has been expressed as one of the reasons that highest performance obtained by the trapezoidal tube.

If there is limiting space for heat exchanger and need to reduce the size (or length) and weight of the heat exchanger, these grooved tubes are suitable. Since, using the grooved tubes increases the heat transfer, it is possible to use a shorter length of the tube to obtain the same heating effects of a longer smooth tube.

Nomenclature

A – heat transfer surface area, [m^2]
C_p – specific heat capacity, [$kJkg^{-1}K^{-1}$]
D – inner diameter of test tube, [m]
e – total energy
f – friction factor, [–]
h – convective heat transfer co-efficient, [$Wm^{-2}K^{-1}$]
$\vec{I}$ – unit vector
K – thermal conductivity of water, [$Wm^{-1}K^{-1}$]
k – turbulent kinetic energy, [Jkg^{-1}]
L – length of test tube, [m]
m – mass flow rate of water, [kgs^{-1}]
n – number of grooves in the tube
Nu – Nusselt number (= hD/K), [–]
Pr – Prandtl number (= $C_p\mu/k$), [–]
ΔP – pressure drop, [Pa]
q – heat transfer rate, [W]
R – resistance
Re – Reynolds number (= VD/ν) [–]
t – temperature, [K]
$\vec{u}$ – velocity vector, [ms^{-1}]
V – mean velocity at the inlet of the tube, [ms^{-1}]

Greek symbols

η – thermal hydraulic performance
ε – dissipation rate of k, [Wkg^{-1}]
μ – viscosity, [Pa·s]
μ_t, μ_{eff} – turbulent effective viscosity, [Pa·s]
ν – kinematics viscosity, [m^2s^{-1}]
ρ – density of water, [kgm^{-3}]
$\bar{\bar{\tau}}_{eff}$ – stress tensor, [Pa]

Subscripts

b – mean
eff – effective
i – inlet
o – outlet
t – turbulent
w – wall
0 – plain tube

Abbreviations

CFD – computational fluid dynamics
RNG – random number generation

References

[1] Aubin, J., *et al*., Modeling Turbulent Flow in Stirred Tanks with CFD: The Influence of the Modeling Approach, Turbulence Model and Numerical Scheme, *Int. J. Experimental Thermal and Fluid Science, 2* (2004), 5, pp. 431-445
[2] Rahimi, M., *et al.*, Experimental and CFD Studies on Heat Transfer and Friction Factor Characteristics of a Tube Equipped with Modified Twisted Tape Insert, *Int. J.Chemical Engineering and Processing, 48* (2009), 3, pp. 762-770
[3] Bilen, K., *et al*., The Investigation of Groove Geometry Effect on Heat Transfer for Internally Grooved Tubes, *Int.J.Applied Thermal Engineering, 29* (2009), 4, 753-761
[4] Kumar, S., Saini, R. P., CFD Based Performance Analysis of a Solar Air Heater Duct Provided with Artificial Roughness, *Int.J.Renewable Energy, 3*4 (2009), 5, pp. 1285-1291
[5] Xiong, R., Chung, J. N., A New Model for Three-Dimensional Random Roughness Effect on Friction Factor and Heat Transfer in Micro Tubes, *Int. J. Heat and Mass Transfer, 53* (2010), 15-16, pp. 3284-3291
[6] Craft, T. J., *et al*., Modeling of Three-Dimensional Jet Array Impingement and Heat Transfer on a Concave Surface, *Int. J. Heat and Fluid Flow, 29* (2008), 3, pp. 687-702
[7] Iacovides, H., *et al*., Flow and Heat Transfer in Straight Cooling Passages with Inclined Ribs on Opposite Walls: an Experimental and Computational Study, *Int.J. Experimental and Thermal Fluid Science, 27* (2003), 3, pp. 283-294
[8] Chaube, A., *et al*., Analysis of Heat Transfer Augmentation and Flow Characteristics Due to Rib Roughness over Absorber Plate of a Solar Air Heater, *Int. J.Renewable Energy , 31* (2006), 3, pp. 317-331
[9] Karagoz, I., Kaya., F., CFD Investigation of the Flow and Heat Transfer Characteristics in a Tangential Inlet Cyclone, *Int. J. Communications in Heat and Mass Transfer, 34* (2007), 9-10, pp. 1119-1126
[10] Rigby, G. D., Evans, G. M., CFD Simulation of Gas Dispersion Dynamics In Liquid Cross Flows, *Int. J. Applied Mathematical Modeling, 22* (1998), 10, pp. 799-810

[11] Li, L., *et al.*, Numerical Study of Periodically Fully-Developed Convection in Channels with Periodically Grooved Part, *Int. J. Heat and Mass Transfer, 51* (2008), 11-12, pp. 3057-3065
[12] Eiamsa-Ard, S., *et al*., 3D Numerical Simulation of Swirling Flow and Convective Heat Transfer in a Circular Tube Induced by Means of Loose Fit Twisted Tapes, *Int. J. Communications in Heat Mass Transfer, 36* (2009), 9, pp. 947-955
[13] Zimparov, V., Prediction of Friction Factors and Heat Transfer Coefficient for Turbulent Flow of Corrugated Tubes Combined with Twisted Tape Inserts, Part 1 – Friction Factors, *Int. J. Heat and Mass Transfer, 47* (2004), 3, pp. 589-599
[14] Zimparov, V., Prediction of Friction Factors and Heat Transfer Coefficient for Turbulent Flow of Corrugated Tubes Combined with Twisted Tape Inserts, Part 2 – Heat Transfer Coefficient, *Int. J. of Heat and Mass Transfer, 47* (2004), 2, pp. 385-393
[15] Goto, M., *et al*., Condensation Heat Transfer of R410A Inside Internally Grooved Horizontal Tubes, *Int. J. Refrigeration, 24* (2001), 7, pp. 628-638
[16] Goto, M., *et al*., Condensation Heat Transfer of R410A Inside Internally Grooved Horizontal Tubes, *Int. J Refrigeration, 26* (2003), 4, pp. 410-416
[17] Promvonge, P., Thermal Enhancement in a Round Tube with Snail Entry and Coiled – Wire Inserts, *Int. J. International Communications in Heat and Mass Transfer, 35* (2008), 5, pp. 623-629
[18] Promvonge, P., Thermal Augmentation in Circular Tube with Twisted Tape and Wire Coil Turbulators, *Int. J. Energy Conversion and Management, 49* (2008), 11, pp. 2949-2955
[19] Chiu, Y-W., Jang., J.-Y., 3D Numerical and Experimental Analysis for Thermal-Hydraulic Characteristics of Air Flow Inside a Circular Tube with Different Tube Inserts, *Int. J. Applied Thermal Engineering, 29* (2009), 2-3, pp. 250-258
[20] Zhang, X., *et al.*, Heat Transfer Characteristics for Evaporation of R417A Flowing Inside Horizontal Smooth and Internally Grooved Tubes, *Int. J. Energy Conversion and Management, 49* (2008), 6, pp. 1731-1739
[21] Li, X.-W., *et al*., Turbulent Flow and Heat Transfer in Discrete Double Inclined Ribs Tube, *Int. J. Heat and Mass Transfer, 52* (2009), 3-4, pp. 962-970
[22] Karwa, R., *et al*., Heat Transfer Coefficient and Friction Factor Correlations for the Transitional Flow Regime in Rib Roughened Rectangular Ducts, *Int. J. Heat and Mass Transfer, 61* (1999), 1, pp. 1597-1615
[23] Karwa, R., Experimental Studies of Augmented Heat Transfer and Friction in Asymmetrically Heated Rectangular Ducts with Ribs on the Heated Wall in Transverse, Inclined, V-Continuous and V-Discrete Pattern, *Int. J. Communication in Heat and Mass Transfer, 30* (2003), 2, pp. 241-250
[24] Tanda, G., Heat Transfer in Rectangular Channels with Transverse and V-Shaped Broken Ribs, *Int. J. Heat and Mass Transfer, 47* (2004), 2, pp. 229-243
[25] Vicente, P. G., *et al*., Experimental Investigation on Heat and Frictional Characteristics of Spirally Corrugated Tubes in Turbulent Flow at Different Prandtl Numbers, *Int. J. Heat and Mass Transfer, 47* (2004), 4, pp. 671-681
[26] Garcia, A., *et al.*, Experimental Study of Heat Transfer Enhancement with Wire Coil Inserts in Laminar-Transition-Turbulent Regimes at Different Prandtl Numbers, *Int. J. Heat Mass Transfer, 48* (2005), 21-22, pp. 4640-4651
[27] Wang, L., Sunden, B., Performance Comparison of Some Tube Inserts, *Int. J. Communication in Heat and Mass Transfer, 29* (2002), 1, pp. 45-56
[28] Zimparov, V., Enhancement of Heat Transfer by a Combination of Three Start Spirally Corrugated Tubes with a Twisted Tape, *Int. J. Heat Transfer, 44* (2001), 3, pp. 551-574
[29] Kothandaraman, C. P., Subramanyan, S., *Heat and Mass Transfer data Book*, New Age International Publishers, New Delhi, 2010
[30] ***, Fluent 6.3 ® April 7(2009)

Paper submitted: April 4, 2011
Paper revised: July 21, 2012
Paper accepted: January 16, 2013